

Synthesis and characterization of nano-sized Mn–TiO₂ catalysts and their application to removal of gaseous elemental mercury

Jiangkun Xie · Naiqiang Yan · Shijian Yang ·
Zan Qu · Wanmiao Chen · Wenqi Zhang ·
Kaihua Li · Ping Liu · Jinping Jia

Received: 9 April 2012 / Accepted: 19 April 2012 / Published online: 8 May 2012
© Springer Science+Business Media B.V. 2012

Abstract To prepare suitable materials for capture of mercury from coal-fired flue gas, nano-sized Mn–TiO₂ catalysts with different manganese loadings were synthesized by use of the template method. Catalytic oxidation performance in the removal of elemental mercury on these catalysts was tested over a wide range of temperature (150–350 °C). Powder X-ray diffraction, N₂ adsorption, and transmission electron microscopy were used to characterize the catalysts. Results showed that Mn–TiO₂ with 10 % manganese content could remove up to 95 % of elemental mercury (balanced with air) at rather high gas space velocity ($1.5 \times 10^5 \text{ h}^{-1}$). It was found that SO₂ inhibited removal of elemental mercury by the catalysts whereas NO had a promoting effect. HCl was also observed to slightly inhibit conversion of mercury on the catalysts. The manganese loading had an important effect on the catalytic oxidation of elemental mercury. With increasing manganese content, the performance of the catalysts in removal of elemental mercury improved. Mn–TiO₂ (10 %) was up to 95 % efficient at removal of elemental mercury in the temperature range investigated.

Keywords Manganese · Mercury removal · Catalytic oxidation · Nano-sized TiO₂

Introduction

Mercury is one of the most hazardous air pollutants because of its neurological toxicity, volatility, bioaccumulation, and persistence [1, 2]. Mercury from anthropogenic activity makes large contribution to global mercury emission in both developed and developing countries [3]. Currently, coal-fired power plants are regarded as the largest single known source of anthropogenic mercury emissions; control of mercury emission is of great significance to human health [4].

J. Xie · N. Yan (✉) · S. Yang · Z. Qu · W. Chen · W. Zhang · K. Li · P. Liu · J. Jia
School of Environmental Science and Engineering, Shanghai Jiao Tong University, Shanghai
200240, China
e-mail: nqyan@sjtu.edu.cn

Mercury in coal-fired flue gas generally occurs in three forms [5, 6], elemental mercury (Hg^0), gaseous oxidized mercury (Hg^{2+}), and particle-bound mercury (Hg^p). Their distributions depend on coal composition and combustion conditions. Because Hg^0 is neither soluble in water nor easily captured by ESP or bag filters, it is difficult to remove by use of current pollution-control devices. However, most Hg^{2+} can be efficiently removed by wet flue gas desulfurization, because of its high solubility, and Hg^p can be effectively captured, with fly ash, by use of electrostatic precipitators (ESP) or bag filters. Thus, oxidation of elemental mercury could greatly enhance the efficiency of mercury capture by currently available pollution-control devices, for example wet desulfurization.

At temperatures below 450 °C, nearly all mercury should be oxidized to Hg^{2+} at chemical equilibrium [7], but catalysts are required to accelerate the oxidation processes, which are often slow because the gas-phase reactions involved are kinetically limited. Many transition metal oxides supported on different carriers, for example Al_2O_3 and TiO_2 , have been observed to aid catalytic oxidation of elemental mercury in the presence of HCl [8–11]. Pinto et al. reported that manganese dioxide on TiO_2 as support had activity in the catalytic oxidation of elemental mercury by the Mars–Maessen mechanism [12]. In most of this work, catalysts were prepared by the impregnation method; metal oxides acted as active sites for catalytic reaction and the supports provided a high surface area to maximize contact between the gaseous mercury and the catalyst [13]. It is worth noting that interaction between the active sites and supports is very important for catalytic reaction. It has been reported that interaction of MnO_x with TiO_2 in the anatase phase is stronger than that with the rutile phase [14]. In general, appropriate active sites, high-surface-area supports, and their interaction are important to the activity of the catalysts.

Most of the catalysts previously used for mercury conversion have been prepared by impregnation of commercially available supports, however, and the interaction of the two may not optimum for the purpose of catalysis. In this study a one-step method was used to synthesize the catalysts; this may lead to different catalytic performance from the impregnation method. Manganese was selected as the active component, anatase phase TiO_2 was synthesized as bulk support material, and the template method was used to synthesize nano-sized Mn/ TiO_2 anatase catalysts to increase the surface area. To achieve better dispersion, instead of post-impregnation, manganese was simultaneously added into the synthetic process. The catalytic activity in the oxidation of elemental mercury was measured by use of packed bed experiments. The effects of flue gas components, for example SO_2 , NO, and HCl were investigated, and the effect of manganese loading at different temperatures was also studied. The results from characterization are discussed here, as also is the mechanism of catalytic oxidation of elemental mercury over the catalysts.

Materials and methods

Titanium-based catalyst preparation

Catalysts were synthesized in accordance with the literature, with some modification [15]. Specific amounts of manganese nitrate (0.1, 0.5, or 1 mmol), 10 mmol

tetrabutyl titanate (Ti(OBu)₄), 40 mmol acetic acid, 24 mmol hydrochloric acid and 2 g F127 (triblock copolymer EO₁₀₆–PO₇₀–EO₁₀₆) were dissolved in 30 ml ethanol. The mixture was stirred vigorously for 1 h. The ethanol was evaporated at 40 °C for 12 h, and the mixture was aged at 65 °C for an additional 24 h. As-synthesized material was calcined at 400 °C in air for 5 h (ramp rate 2 °C min⁻¹) to obtain nano-sized Mn–TiO₂ catalyst. The catalysts are denoted Mn–TiO₂ (*x* %), where *x* % denotes the molar ratio percentage of manganese to titanium.

For comparison, Mn–P25 (10 %) was prepared by the impregnation method (manganese to titanium molar ratio 10:100) and calcined at 400 °C for 5 h. All the synthesized catalysts were ground to 40–60 mesh particles for testing.

Catalyst characterization

Powder X-ray diffraction patterns (PXRD) were obtained by use of a Rigaku D/max-2200/PC powder diffractometer using Cu K α radiation (40 kV and 20 mA). A glass holder was used to support the samples. The scanning range was from 10° to 80° with scanning velocity 7° min⁻¹. The XRD phases present in the samples were identified by use of JCPDS data file no. 21–1272. The microstructure of the catalysts was analyzed by transmission electron microscopy. Samples were dispersed in ethanol with strong sonication before analysis, and the data were collected on a JEM-2100 (20 kV). Nitrogen adsorption and desorption isotherms were obtained on a nitrogen-adsorption apparatus (Quantachrome Nova 2200e) at –196 °C (temperature of liquid nitrogen bath). All samples were degassed for 3 h at 300 °C before testing. Specific surface areas were calculated by use of the Brunauer–Emmett–Teller (BET) method; pore volume and average pore size were calculated by use of the Barrett–Joyner–Halenda (BJH) model. X-ray photoelectron spectroscopy (XPS) measurements were obtained by use of a Thermo (Escalab 250) spectrometer with Al K α as the excitation source. The C 1s line at 284.6 eV was taken as a reference for binding energy calibration. Temperature program reduction (TPR) experiments were carried out on a AutoChem II 2920. Approximately 120-mg samples were tested by increasing the temperature from 50 to 650 °C. A mixture of 10 vol% H₂ in N₂, with a continuous temperature ramp, was used to reduce the catalyst. Samples were degassed for 1 h at 250 °C under He atmosphere before testing.

Activity measurement

The assembly used for capture of elemental mercury consisted of an elemental mercury permeation tube, a packed-bed reactor, a cold-vapor atomic absorption spectrometer (CVAAS), and an online data-acquisition system. Air was used as the carrier gas to yield a stable concentration of elemental mercury. A tubular furnace was used to control the reactor at the desired temperatures. Initially, Air bypassed the mercury permeation tube through a blank tube to determine the baseline; gas containing elemental mercury was then diverted to blank or reactor to determine initial elemental mercury signals. The process flow of packed bed experiments has been reported elsewhere [4]. A given amount of catalyst was inserted in the middle

of the column reactor; the reactor was then packed with quartz wool to support the catalyst layer and prevent its loss.

Elemental mercury removal tests were performed with an inlet gas stream flow of 0.7 l min^{-1} containing $130 (\pm 10) \mu\text{g m}^{-3}$ elemental mercury which was balanced with air. Studies were conducted in the temperature range 150 to 350 °C. Catalyst (20 mg) was placed in the fixed bed for each experiment. (The gas space velocity was approximately $1.5 \times 10^5 \text{ h}^{-1}$). To test the effect of flue gas components, 400 ppm SO_2 , 300 ppm NO , 10 ppm HCl , or their mixture was introduced into the inlet gas. The concentrations of elemental mercury in the influent and effluent were continuously measured by a CVAAS (SG921; Jiangfen, China) which was calibrated by use of a Lumex RA 915+ mercury analyzer. The Hg^0 removal efficiency (η) was calculated as follows:

$$\eta = \frac{\text{Hg}_{\text{inlet}}^0 - \text{Hg}_{\text{outlet}}^0}{\text{Hg}_{\text{inlet}}^0} \times 100\% \quad (1)$$

where $\text{Hg}_{\text{inlet}}^0$ and $\text{Hg}_{\text{outlet}}^0$ denote the inlet and outlet concentrations, respectively, of elemental mercury.

To investigate the effect of flue gas components, the area of the breakthrough curve of elemental mercury on Mn-TiO_2 ($x \%$) at 300 °C during the test time (6 h) was integrated and the adsorption capacity for mercury was calculated from the flow rate. Adsorption capacity was defined as the mass of elemental mercury converted into HgO or other forms on unit mass of catalyst. In this experiment it was calculated as follows:

$$Q = \frac{1}{m} \int_{t_0}^{t_1} (\text{Hg}_{\text{inlet}}^0 - \text{Hg}_{\text{outlet}}^0) \times f \times dt \quad (2)$$

where Q is the adsorption capacity, m is mass of catalyst (20 mg in this experiment), f denotes the flow rate of the influent, and t_0 and t_1 represent the initial and final test times, respectively, of the breakthrough curves.

Results and discussion

Catalytic performance

Activity

The efficiency of removal of elemental mercury on TiO_2 and on Mn-TiO_2 with different manganese loadings, at temperatures from 150 to 350 °C, is illustrated in Fig. 1. It was found that the efficiency of removal of elemental mercury by commercial powdered TiO_2 (P25) was very poor at the temperatures investigated. TiO_2 synthesized by use of the template method removed elemental mercury more efficiently than commercial TiO_2 powder (P25), but the efficiency was still below 60 %. The larger specific surface area of synthesized TiO_2 compared with P25 may be one explanation of the more efficient capture of Hg^0 . Analysis indicated that P25

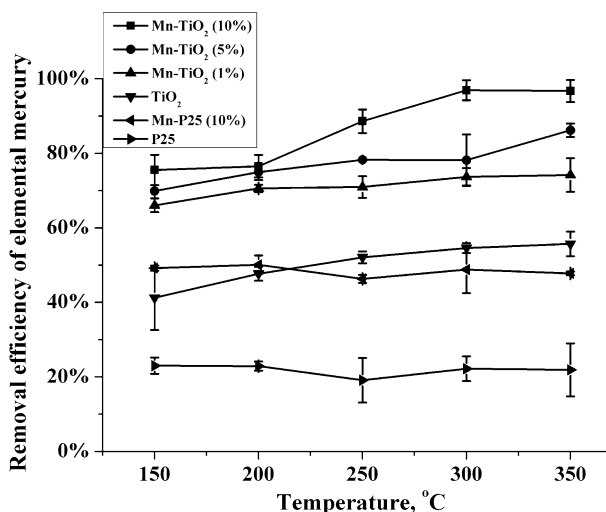


Fig. 1 Efficiency of removal of elemental mercury by titanium-based catalysts (elemental mercury concentration, $130 \pm 10 \mu\text{g m}^{-3}$ (balanced with air); mass of catalyst, 20 mg; gas space velocity, $1.5 \times 10^5 \text{ h}^{-1}$)

was a mixture of anatase and rutile phases (approx. 80:20), but that TiO₂ synthesized by use of the template method was mainly the uniform anatase phase. The anatase phase of TiO₂ is commonly regarded as more active than the rutile phase; this may be another explanation of the greater efficiency of removal by the synthesized TiO₂ [14]. As illustrated in Fig. 1, with increasing manganese content, Hg⁰ capture efficiency increased significantly, especially at relatively high temperature. At 300 and 350 °C, up to 95 % Hg⁰ removal efficiency could be achieved over Mn-TiO₂ (10 %) catalyst. Furthermore, this high removal efficiency on Mn-TiO₂ (10 %) was maintained during the test period (6 h) whereas the efficiency of removal on Mn-TiO₂ (1 %) decreased gradually after approximately 3 h. This indicated that manganese was the active site and its loading on the catalyst was important for catalytic oxidation of gaseous elemental mercury. To compare the performance of the synthesized catalysts with the P25-based catalyst, Mn-P25 (10 %) was prepared by the impregnation method. As illustrated in Fig. 1, the efficiency of removal of elemental mercury over Mn-P25 was approximately 50 % in the range of temperatures tested. This efficiency is higher than that of pure P25 but much lower than that of synthesized Mn-TiO₂ catalysts.

Effect of SO₂, NO, and HCl on Mn-TiO₂ (10 %) catalysts

To study the effect of flue gas components on removal of elemental mercury, SO₂, NO, HCl, or their mixture was used to simulate the flue gas. Because high removal efficiency can be readily achieved at 300 °C, this temperature was chosen to investigate the effect of flue gas components. Breakthrough curves for elemental mercury on Mn-TiO₂ with different manganese loadings were obtained at 300 °C.

The areas were integrated and transformed to calculate the adsorption capacities of mercury on these catalysts in accordance with Eq. (2). In general, addition of SO_2 inhibited conversion of elemental mercury whereas NO promoted its oxidation on the catalysts (Fig. 2). It is speculated that SO_2 was competitively adsorbed on the active site and prevented contact of mercury molecular with Mn– TiO_2 . This inhibition effect of SO_2 is consistent with the published literature [12]. The promoting effect of NO may be attributed to its gaseous reaction with elemental mercury, because NO was observed to slightly oxidize elemental mercury in the presence of oxygen at 300 °C. HCl had a slightly negative effect on conversion of elemental mercury, so the Deacon process (in which HCl is catalytically oxidized into Cl_2 on the surface of catalyst) may be not the mechanism responsible for oxidation of elemental mercury on synthesized Mn– TiO_2 catalysts. Furthermore, the efficiency of removal of elemental mercury on the catalysts did not decrease significantly in simulated flue gas (containing SO_2 , NO, and HCl).

Characterization results

Physical properties

The BET specific surface areas, pore volume, and average pore diameter of TiO_2 and Mn– TiO_2 (1–10 %) are summarized in Table 1. BET surface area of synthesized TiO_2 was much higher than that of commercial P25, and this could be one explanation of its better performance in removal of mercury than that of P25. As shown in Table 1, addition of manganese to TiO_2 slightly affected its physical properties. Addition of manganese during the synthetic process reduced the catalysts' BET surface area to some extent, but the decrease was not directly dependent on manganese loading. This illustrated that addition of manganese (up to 10 % molar ratio of Mn to Ti) did not significantly change the microstructure or

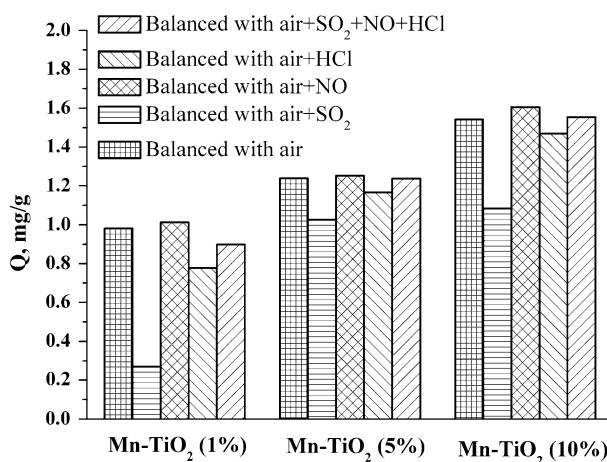


Fig. 2 Effect of SO_2 , NO, or HCl on mercury adsorption capacity of Mn– TiO_2 catalysts at 300 °C during 6 h (test conditions: SO_2 400 ppm, NO 300 ppm, HCl 10 ppm, gas space velocity: $1.5 \times 10^5 \text{ h}^{-1}$)

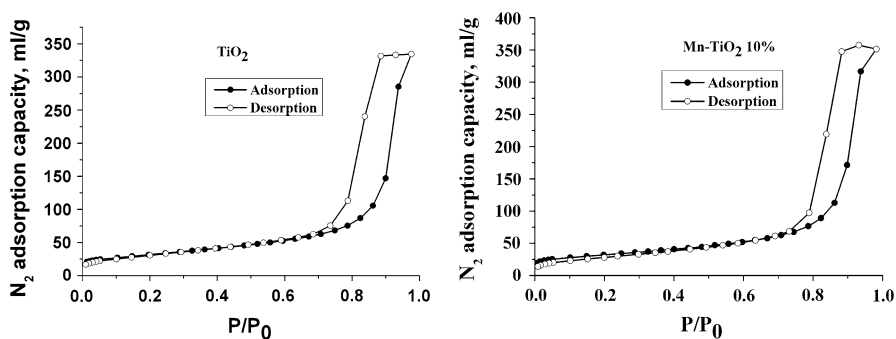
Table 1 Physical properties of P25, Mn-P25 (10 %), TiO₂, and Mn-TiO₂ catalysts with different manganese loadings

Sample	BET surface (m ² g ⁻¹)	Pore volume (cm ³ g ⁻¹)	Average pore diameter (nm)
P25	45	0.263	24.384
Mn-P25 (10 %)	44	0.246	19.502
TiO ₂	113	0.567	11.523
Mn-TiO ₂ (1 %)	93	0.614	15.595
Mn-TiO ₂ (5 %)	104	0.653	15.706
Mn-TiO ₂ (10 %)	113	0.606	11.569

increase the particle size of the synthesized TiO₂, and this was confirmed by TEM and XRD analysis (below). Furthermore, as displayed in Fig. 3, for both TiO₂ and Mn-TiO₂ (10 %) there was significant hysteresis between adsorption and desorption isotherms, which is usually an indication of mesoporous materials, (Such hysteresis loops were also found in isotherms of Mn-TiO₂ with 1 and 5 % manganese loadings; the diagrams are not shown here.) This illustrated that a mesoporous structure was formed by aggregation of nano-particles. This mesoporous structure may facilitate mass transfer in the catalytic reaction.

PXRD characterization

The PXRD patterns of TiO₂ and Mn-TiO₂ (1–10 %) calcined at 400 °C are shown in Fig. 4. It is apparent all the samples afforded broad diffraction lines attributable to the anatase phase of TiO₂ (JCPDS file no. 21-1272). No significant peaks could be attributed to the rutile phase or MnO_x. In combination with the BET characterization results, MnO_x could be speculated to be highly dispersed or present as an amorphous phase on the surface of catalysts. It is apparent from Fig. 4 that addition of manganese to the TiO₂ affected the signal intensities of the anatase phase. With increasing manganese content, peak intensities of the anatase phase decreased slightly but peaks corresponding to MnO_x were still not observed when the molar proportion of manganese to titanium was as high as 10 %. This illustrates that anatase was a uniform phase in the synthesized catalysts, and this uniform

**Fig. 3** N₂ adsorption and desorption isotherms of TiO₂ and Mn-TiO₂ (10 %)

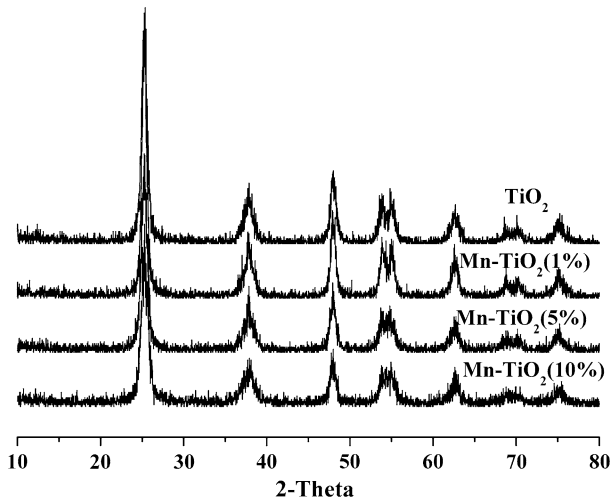


Fig. 4 PXRD diagrams of synthesized TiO_2 and Mn-TiO_2 catalysts

anatase phase may benefit its catalytic activity. Thus, this phase difference may be another reason synthesized TiO_2 performed better at mercury removal than commercial P25.

TEM characterization

As shown in Fig. 5, TiO_2 and Mn-TiO_2 catalysts synthesized with the assistance of the template agent were nano-sized particles. Comparison of the two images shows that addition of manganese during the synthetic process did not significantly change the particle size of the synthesized catalysts. Additionally, no new crystal phase could be observed in TEM diagram. Thus, it can be speculated that manganese was highly dispersed in the catalyst or was present as an amorphous phase. This speculation is consistent with the results from PXRD. Interestingly, the mesoporous structure shown by the hysteresis loop of the adsorption and desorption curves was

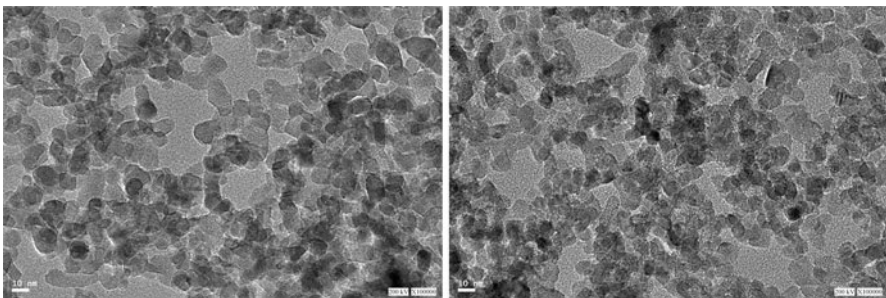


Fig. 5 TEM diagrams of TiO_2 (left) and Mn-TiO_2 (10 %) (right)

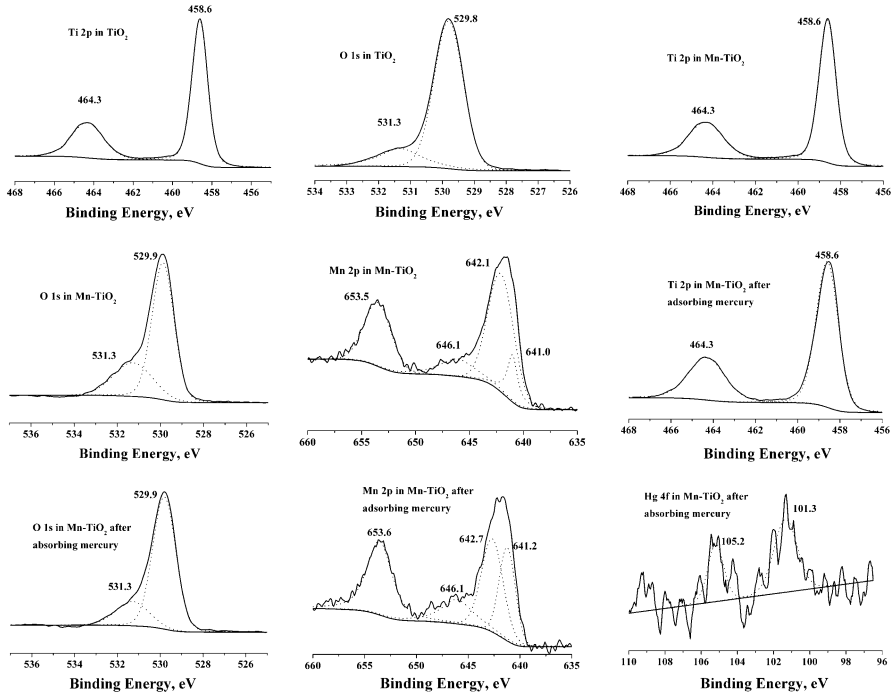


Fig. 6 XPS spectra of TiO₂, Mn–TiO₂ (10 %), and Mn–TiO₂ (10 %) after adsorbing mercury

not clearly observed here. It is possible that sonication of the sample before TEM destroyed the mesoporous structure formed by particle aggregation.

XPS characterization

Information about the surface of the catalysts (TiO₂, Mn–TiO₂, and Mn–TiO₂ after adsorbing mercury) was obtained by XPS characterization. XPS spectra over the spectral regions Ti 2*p*, O 1*s*, Mn 2*p*, and Hg 4*f* are displayed in Fig. 6.

For the synthesized TiO₂, peaks at 464.3 and 458.6 eV were assigned to Ti 2*p* 1/2 and Ti 2*p* 3/2 of Ti⁴⁺. The O 1*s* mainly centered at approximately 529.8 eV, another relatively weak peak at 531.1 eV was assigned to hydroxyl (–OH) [16, 17].

For the synthesized Mn–TiO₂ (10 %), peaks corresponding to Ti 2*p* and O 1*s* appeared at almost the same binding energy as TiO₂. Peaks at about 642.1 and 641.0 eV could be attributed to Mn 2*p* 3/2 of Mn⁴⁺ and Mn³⁺, respectively. Their corresponding peaks of 2*p* 1/2 overlapped and appeared at 653.5 eV. Combined with the binding energy of O 1*s*, manganese could exist mainly as amorphous MnO₂ in the fresh catalyst.

For the spent catalyst, the area of the peak at 642.7 eV (corresponding to Mn 2*p* 3/2 of Mn⁴⁺) decreased whereas the area of the peak at 641.2 eV (corresponding to Mn 2*p* 3/2 of Mn³⁺) increased significantly. The increased Mn³⁺ content of the surface of the spent catalyst is clearly apparent from Table 2. Moreover, peaks

Table 2 XPS results for TiO₂, Mn–TiO₂ (10 %), and spent Mn–TiO₂ (10 %) catalysts

Sample	Surface atomic concentration (%)			
	Ti ⁴⁺	O	Mn ⁴⁺	Mn ³⁺
TiO ₂	32.87	67.13	–	–
Mn–TiO ₂ (10 %)	21.35	65.20	10.83	2.62
Spent Mn–TiO ₂ (10 %)	22.67	65.77	6.15	5.41

corresponding to Hg 4f 7/2 at 101.3 eV and Hg 105.2 eV were also observed in the spectra. It can be concluded that part of the Mn⁴⁺ was reduced to Mn³⁺ whereas Hg was oxidized to Hg²⁺. This result supports the hypothesis that oxidation of the elemental mercury proceeded via the Mars–Maessen mechanism. According to this mechanism, gaseous elemental mercury first collides with the surface of the catalyst and is adsorbed. The adsorbed elemental mercury is then oxidized to mercury oxide by manganese dioxide and the manganese dioxide is reduced to manganese sesquioxide. The mercury oxide subsequently reacts with the catalyst to form a binary oxide.

H₂-TPR characterization

The effect of preparation procedure on oxidation ability was studied by TPR analysis with H₂ as reducer. As shown in Fig. 7, the reduction behavior of Mn–P25 was different from that of synthesized Mn–TiO₂ catalysts. Two reduction peaks were observed in the range 200–400 °C for the Mn–P25 catalyst. Peaks at 279 and 336 °C could be attributed to reduction of MnO₂ to Mn₂O₃ and Mn₂O₃ to Mn₃O₄. For the Mn–TiO₂ catalyst, three reduction peaks were observed in the range 200–500 °C [18]. The peak at 307 °C corresponded to reduction of MnO₂ to Mn₂O₃ and the peak at 376 °C could be attributed to reduction of Mn₂O₃ to Mn₃O₄. A peak for reduction of Mn₃O₄ to MnO was observed at 438 °C, but this was not observed in the reduction behavior of Mn–P25. In general, the positions of the reduction peaks for Mn–TiO₂ were, to some extent, shifted toward higher temperature compared with those for Mn–P25; this indicates that Mn on Mn–P25 was more easily reduced than Mn on the Mn–TiO₂ catalyst. The activity results for the catalysts show, however, that this slightly different oxidation behavior was not the most critical aspect of the catalytic activity.

Conclusions

Nano-sized Mn–TiO₂ catalysts with different manganese loadings had been synthesized, characterized, and evaluated for effective removal of gaseous elemental mercury in simulated flue gas. Activity measurements indicated that up to 95 % of elemental mercury could be removed over Mn–TiO₂ catalyst at 300 and 350 °C. SO₂ inhibited removal of elemental mercury whereas NO had a promotional effect. HCl also slightly inhibited conversion of mercury on the

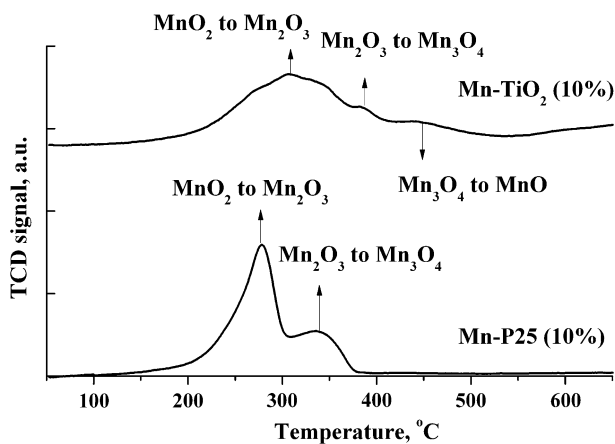


Fig. 7 H₂-TPR diagrams for Mn-P25 and Mn-TiO₂ (10 %)

synthesized catalysts. The surface area of the catalysts was not the main factor determining removal of elemental mercury. Manganese loading seemed to have a much greater effect on efficiency. PXRD and TEM analysis indicated the MnO_x was highly dispersed or existed as an amorphous phase on the surface of the catalyst. XPS and H₂-TPR results suggested that MnO₂ was the main form of manganese in the fresh catalysts, which may benefit catalytic oxidation of gaseous elemental mercury.

Highlights

- 95 % Hg⁰ removal efficiency could be achieved by use of the Mn-TiO₂ nano-composite.
- Manganese loading affected the performance of the nano-composites.
- High surface area and uniform anatase phase are important aspects of its high removal efficiency.

Acknowledgments This study was supported by the National Natural Foundation of China (21077073, 50908145) and the National High-Tech Research and Development Program (863) of China (2011AA060801). Dr Yongfu Guo, Yongpeng Ma, Bing Pei, and Fei Liu are thanked for their helpful advice.

References

1. W.F. Fitzgerald, C.H. Lamborg, C.R. Hammerschmidt, *Chem. Rev.* **107**, 641 (2007)
2. D.G. Streets, Q. Zhang, Y. Wu, *Environ. Sci. Technol.* **43**, 2983 (2009)
3. G.B. Jiang, J.B. Shi, X.B. Feng, *Environ. Sci. Technol.* **40**, 3672 (2006)
4. S.J. Yang, Y.F. Guo, N.Q. Yan, D.Q. Wu, H.P. He, J.K. Xie, Z. Qu, C. Yang, J.P. Jia, *Chem. Commun.* **46**, 8377 (2010)
5. C.E. Romero, Y. Li, H. Bilirgen, N. Sarunac, E.K. Levy, *Fuel* **85**, 204 (2006)

6. N.Q. Yan, Z. Qu, Y. Chi, S.H. Qiao, R.L. Dod, S.G. Chang, C. Miller, *Environ. Sci. Technol.* **43**, 5410 (2009)
7. A.A. Presto, E.J. Granite, *Environ. Sci. Technol.* **40**, 5601 (2006)
8. W.J. Lee, G.N. Bae, *Environ. Sci. Technol.* **43**, 1522 (2009)
9. J.F. Li, N.Q. Yan, Z. Qu, S.H. Qiao, S.J. Yang, Y.F. Guo, P. Liu, J.P. Jia, *Environ. Sci. Technol.* **44**, 426 (2010)
10. S.H. Qiao, J. Chen, J.F. Li, Z. Qu, P. Liu, N.Q. Yan, J.Q. Jia, *Ind. Eng. Chem. Res.* **48**, 3317 (2009)
11. Q. Wan, L. Duan, K.B. He, J.H. Li, *Chem. Eng. J.* **170**, 512 (2011)
12. L. Ji, P.M. Sreekanth, P.G. Smirniotis, S.W. Thiel, N.G. Pinto, *Energy Fuels* **22**, 2299 (2008)
13. E.J. Granite, H.W. Pennline, R.A. Hargis, *Ind. Eng. Chem. Res.* **39**, 1020 (2000)
14. P.R. Ettireddy, N. Ettireddy, S. Mamedov, P. Boolchand, P.G. Smirniotis, *Appl. Catal. B Environ.* **76**, 123 (2007)
15. J. Fan, S.W. Boettcher, G.D. Stucky, *Chem. Mater.* **18**, 6391 (2006)
16. T. Herranz, S. Rojas, M. Ojeda, F.J. Perez-Alonso, P. Terreros, K. Pirota, J.L.G. Fierro, *Chem. Mater.* **18**, 2364 (2006)
17. Y. Zhang, M. Yang, X.M. Dou, H. He, D.S. Wang, *Environ. Sci. Technol.* **39**, 7246 (2005)
18. F. Kapteljn, L. Singoredjo, A. Andreini, J.A. Moulijn, *Appl. Catal. B Environ.* **3**, 173 (1994)